Journal of Materials Chemistry A

ROYAL SOCIETY OF CHEMISTRY

PAPER

View Article Online
View Journal | View Issue

Cite this: J. Mater. Chem. A, 2025, 13, 32528

Bioinspired poly(catechol sulfide) as organic cathode materials for lithium metal batteries

Nicolas Goujon, *[abc] Juan Cubero-Cardoso, [d] Juan Urbano *[d] and David Mecerreyes [ac]

Received 10th June 2025
Accepted 4th August 2025

DOI: 10.1039/d5ta04701c

rsc.li/materials-a

Novel bio-inspired poly(catechol sulfide) PCS copolymers with mono- and dual-redox properties are proposed for application as organic cathode materials in lithium metal batteries. Poly(catechol sulfide) copolymers were synthesized from naturally abundant catechol and sulfur, limiting their environmental footprint. These copolymers were characterized by FTIR, ^{1}H and ^{13}C NMR, TGA and GPC, confirming the formation of the sulfide linkage between the catechol units and their oligomeric nature. The electrochemical characterization of the PCS copolymers reveals the dual redox activity when a sulfur content of above 25 wt% is present. The catechol redox process exhibits great rate capability and cycling stability, while the sulfur redox process suffers from more sluggish kinetics due to the labile nature of the poly(sulfide) redox process (*i.e.* bond cleavage). Nevertheless, the PCS copolymers with either 25 or 75 wt% sulfur content display great specific energy densities of 237 Wh kg^{-1} and 182 Wh kg^{-1} at specific power densities of 10.17 kW kg^{-1} and 31.18 kW kg^{-1}, respectively. These results highlight the potential of PCS copolymers as sustainable, high power and energy density organic cathode materials for lithium metal batteries.

Introduction

Lithium-ion batteries (LiBs) are considered a key enabler for the decarbonization of the transport sector, with a projected annual battery demand of 3500 gigawatt-hours by 2030 from electromobility applications.[1] In view of the battery volume required to support this technological transition, the sustainability of battery technology is becoming an increasingly important criterion, in addition to traditional performance indicators such as energy density, power density, safety and low cost. This is reflected in the recent legislation about batteries and its waste, aiming at regulating their carbon footprint, recyclability and toxic and/or critical raw material use.[2] Indeed, several key elements for high energy density LiBs, based on lithium nickel manganese cobalt oxides (NMC) cathode chemistry, are already listed in the fourth critical raw material list established by the European Commission in 2020 (*i.e.* lithium, cobalt, nickel and graphite).[3] Consequently, the share of lithium iron phosphate (LFP) battery cathode chemistry in worldwide electric car sales has more than quintupled in the last five years, accounting for 40% in 2023.[1] The renewed popularity of LFP cathode chemistry is driven by its lack of critical raw materials use, lower cost, longer cycle life and improved safety. However, LFP cathode chemistry suffers from 20 to 30% lower energy density, when compared to high nickel content NMC cathode chemistry.[1] Therefore, there is an urgent need for low-cost, critical raw material free and high energy density cathode chemistry alternatives.

In this regard, organic materials represent a great cathode chemistry alternative due to their inherent sustainability (*i.e.* composed of abundant atoms), low-cost and high power and energy densities.[4–6] To date, a wide variety of organic redox chemistries have been explored, including but not exclusively conjugated carbonyls, conjugated thioethers, conjugated amines, and nitroxide radicals, allowing a great versatility towards specific energy storage application requirements. Among organic cathode materials, redox polymers are showing great promise due to their limited solubility in battery electrolytes, when compared to organic cathode materials based on small organic molecules.[4–6] While the tethering of a redox moiety to a polymer backbone has been reported as an effective approach to limit solubility, it comes with a cost in terms of electrode material capacity and thus energy density. Indeed, the capacity that can be reversibly stored and extracted from electrode materials is defined by the number of electrons involved in the redox reaction, normalized by the molecular weight of the unit cell or repeating units for inorganic and organic electrode materials, respectively. As such, the molecular weight of

[a]POLYMAT, University of the Basque Country UPV/EHU, Avenida Tolosa 72, 20018 Donostia-San Sebastián, Spain. E-mail: nicolasjeanchristopher.goujon@ehu.eus
[b]Applied Chemistry Department, Faculty of Chemistry, University of the Basque Country EHU, Manuel Lardizabal Pasealekua, 3, 20018 San Sebastián, Spain
[c]Ikerbasque, Basque Foundation for Science, 48013 Bilbao, Spain
[d]Laboratory of Sustainable and Circular Technology. CIDERTA and Chemistry Department, Faculty of Experimental Sciences. Campus de "El Carmen", University of Huelva, 21071 Huelva, Spain

a polymer backbone and its linker to the redox moiety is considered as "dead weight", increasing the overall molecular weight of the repeating unit and thus lowering the specific capacity of the electrode material based on redox polymer.

Inverse vulcanization, a technique introduced in 2013 by Pyun *et al.*,[7] utilizes elemental sulfur, a byproduct of the petrochemical industry, to synthesize sulfur-rich polymers. This process involves the copolymerization of sulfur with multifunctional alkenes, forming poly(sulfide) bonds that enhance the properties of materials at a low cost due to high atomic efficiency.[8] Sulfur polymers obtained by inverse vulcanization have diverse applications, including contaminant adsorption, battery materials, optical material creation and others.[9] This method not only mitigates environmental impact by using industrial byproducts but also enables the design of polymers with customizable properties.[8] Recently, inverse vulcanization copolymers are gaining attention for enhancing lithium–sulfur battery performance.[10,11] The carbon-sulfur-rich copolymers show improvements of lithium-ion transport, increase sulfur utilization, and mitigate the shuttle effect, which typically shortens lithium–sulfur battery life.[10] The versatility of inverse vulcanization allows for the customization of polymer properties by selecting different comonomers and optimizing synthesis conditions, making these polymers highly adaptable to battery-specific needs. Recent studies have explored various redox active monomers, including ferrocene or anthraquinone units, to create cathode materials with superior characteristics, further advancing the potential of these batteries.[10,12–17]

Catechol groups, ubiquitous in natural systems, play a crucial role in various biological processes and industrial applications.[18] Their chemical reactivity and ability to form hydrogen bonds and electrostatic interactions allow them to interact effectively with diverse surfaces.[19,20] Additionally, catechol-based polymers have been proposed as promising organic cathode materials, *via* the reversible oxidation of enol into ketone.[21–23]

Herein, a novel bio-inspired catechol redox polymer with redox active sulfide linkage (poly(catechol sulfide), PCS) is proposed for application as a high power and energy density organic cathode material for lithium metal batteries. Our goal was to combine in an original polymer, the redox chemistry of poly(sulfide) and catechol units. Through variation of the copolymer composition and the sulfur content, the electrochemistry and redox activity of PCS were investigated. Finally, the cycling performance of the PCS with various compositions was assessed as cathode materials in organic lithium metal batteries.

Experimental

Poly(catechol sulfide) synthesis

The inverse vulcanization process of elemental sulfur (S_8) and catechol was conducted with a slight modification to Chalker's method.[24] S_8 and catechol were heated and melted under vigorous stirring at 170 °C until the desired weight-to-weight (wt/wt) ratio was achieved, called PCS-[sulfur wt%]. Furthermore, the reaction was conducted using a catalytic approach with the inclusion of zinc diethyldithiocarbamate ($Zn(DEDC)_2$) at a concentration of 1% w/w relative to the copolymer.[25] The blends were continuously stirred for 72 hours while maintaining the temperature, facilitating the complete conversion of the comonomers with the refluxed material. Following the formation of the copolymer, a purification step was carried out using tetrahydrofuran (THF) to wash the resulting product.

Structural analysis of poly(catechol sulfide)

Fourier transform infrared (FTIR) spectra were recorded in the absorbance mode within a wavenumber range of 400–4000 cm^{-1} at 4 cm^{-1} resolution using FT/IR-4200 apparatus (Jasco Analytical Instrument, Japan). In the transmission mode, a total of 46 scans were done for each sample. In addition, an attenuated total single reflection (ATR) accessory fitted with a diamond crystal has been used for surface FTIR analyses of the films.

Thermal characterization of copolymers was performed by differential scanning calorimetry to provide information about the homogeneity of the copolymers by detecting any thermal events. Differential Scanning Calorimetry (DSC) measurements were performed with a DSC25 instrument (TA instrument, USA). Heat flow curves were obtained by applying a temperature program of 0 to 180 °C/180 °C to 0 °C/0 to 180 °C, at 10 °C min^{-1}. The significant events were determined from the second scan to cancel the effect of aging on the morphology of the samples.

The thermal resistance of copolymers was studied using thermogravimetric analysis (TGA), which provides information on the thermal decomposition of these systems. TGA was carried out under a N_2 purge (40 mL min^{-1}) using a TGA 8000 instrument (Pekin Elmer) at 10 °C min^{-1}.

The prepared copolymers were also characterized by solution NMR. ^1H and ^{13}C NMR spectroscopy was used to determine the chemical structures of the poly (S/CO) copolymers. Nuclear magnetic resonance spectroscopy (^1H NMR) of copolymer samples was performed at 500 MHz using a Varian Mercury 500 spectrometer. Deuterated pyridine-d_5 was used as a solvent. ^1H and ^{13}C NMR shifts are reported relative to tetramethylsilane.

Electrode formulation

The PCS-based electrodes were prepared using a doctor blade coating method onto a carbon coated aluminum current collector (Gelon energy Co. Limited, 11 μm thick). For this purpose, a slurry of PCS copolymer (20 wt%), conductive carbon (Super C65, Timical, 70 wt%) and binder (PVDF, Solef® 5130, 10 wt%) in *N*-methylpyrrolidone (NMP) was prepared using a speed mixer at a rpm of 3000 for 5 min after each solvent addition (SpeedMixerTM, DAC 300-100-SE). Prior to solvent mixing, all dried components of the slurry were mixed with a ball mill at an rpm of 500 for 5 min (FRITSCH, Planetary Micro Mill PULVERISETTE 7). PCS-based electrodes were dried under high vacuum at 50 °C for 24 h, resulting in an active material loading of around 0.5 mg cm^{-2}.

Electrochemical characterization

Lithium metal batteries using the PCS-based cathodes were assembled inside an argon glovebox using a lithium electrode (Gelon energy Co. Limited, 11 μm thick) and a cathode electrode of diameter 6 mm. Glass microfiber filter (Whatman™, GF/B, 16 mm in diameter) soaked in 1 M LiTFSI in DOL/DME (50/50 vol%) was used as the separator. Cyclic voltammetry (CV) and galvanostatic measurements were performed in a lithium metal coin cell using a multi-channel potentiostat (Biologic, VMP3) or a battery cycler (Neware), respectively.

Results and discussion

Poly(catechol sulfide) synthesis and characterization

An environmentally friendly polymerization method, *via* the catalyzed electrophilic aromatic substitution reaction, was employed to generate the PCS copolymers (Scheme 1). The catalyzed electrophilic aromatic substitution reaction between elemental sulfur and the catechol was performed under solvent-free conditions with 1 wt% of the $Zn(DEDC)_2$ catalyst at 170 °C for 72 hours. By this method, a series of PCS copolymers have been synthesized *via* inverse vulcanization with varying sulfur contents (*i.e.* 25, 50 and 75 wt%) as illustrated in Scheme 1 by varying the monomer feed ratio. The resulting PCS copolymers were insoluble in common organic solvents, such as tetrahydrofuran, chloroform, and dimethyl sulfoxide.

The chemical composition of the PCS copolymers was characterized by means of NMR (nuclear magnetic resonance) and ATR-FTIR (attenuated total reflectance Fourier transform infrared) spectroscopy techniques and the results are shown in Fig. 1. As can be seen in the ^{1}H-NMR spectrum (Fig. 1a), all PCS copolymers display two multiplets are observed at $\delta = 6.60$ and 6.70 ppm, indicating the presence of aromatic ring C–H protons. Change in the multiplicity of the aromatic ring protons, along with their downfield shift, suggests that the catechol has reacted with elemental sulfur. Additionally, a downfield shift is also observed for the proton signal associated with the hydroxyl group of the catechol, suggesting an alteration in its chemical environment, likely resulting from a modification of the aromatic ring. Similar trends are observed in the ^{13}C NMR spectrum (Fig. 1b) of the PCS copolymers, with the presence of both aromatic carbon and aromatic alcohol signals (*i.e.* $\delta = 116$, 119 and 145 ppm), along with a reduction of their intensity as the sulfur content increases. ATR-FITR analysis of the PCS copolymers was also performed, and the results are shown in Fig. 1c. A broad vibration mode in the range of 3000–3500 cm^{-1} is observed for all PCS copolymers, corresponding to phenolic O–H and aromatic C–H stretches from the catechol moiety. Additionally, a characteristic decrease in the transmittance of the PCS copolymers is observed when increasing sulfur content, confirming the successful incorporation of sulfur in the molecular structure of the PCS copolymers.[26–28] Additionally, a vibration mode at 1580 cm^{-1} is observed for all PCS copolymers, characteristic of the C–S stretching vibrations.[29] Overall, both ^{1}H/^{13}C NMR and FTIR spectra confirm the successful incorporation of the catechol moiety within the PCS copolymer chemical composition. Differential scanning calorimetry (DSC) was employed to evaluate the homogeneity of PCS copolymers by identifying thermal transitions. Fig. 1d depicts the heat flow curves obtained for the PCS copolymers and their thermal properties are summarized in Table 1. All PCS copolymers display a glass transition at a temperature ranging from 38 °C to 62 °C depending on the sulfur content. The glass transition temperature of the PCS copolymers decreases as the content of sulfur is increased. This is in agreement with previous reports and is due to the increased flexibility of the C–S–$(S)_n$–C linkage, as n increases, resulting in a lower glass transition temperature.[30,31] Additionally, an endothermic transition is observed at a temperature of 113 °C for the PCS copolymer with the highest sulfur content (*i.e.* PCS-75), which could be associated with the melting of the crystalline long C–S–$(S)_n$–C poly(sulfide) chains in the PCS-75 copolymer.[32,33] Overall, the DSC results confirm the successful reaction of elemental sulfur with catechol to generate stable copolymers.

The thermal stability of PCS copolymers was investigated using thermogravimetric analysis (TGA), providing insights into their thermal behavior. As depicted in Fig. S2a, distinct stages of degradation are evident in the thermal assessment of elemental sulfur and catechol. The loss of sulfur and volatile sulfides, reported by Cubero-Cardoso *et al.*[26] to occur within the temperature range of 204.5–307.6 °C, is observed in all three PCS copolymers under study. Thermal degradation of the PCS copolymers varies depending on the S/catechol ratio, manifesting in multiple degradation peaks. The PCS-50 copolymer exhibits an initial degradation stage occurring within the temperature range of 100 to 180 °C, characterized by accelerated decomposition compared to the other copolymers examined. Another degradation process corresponds to the release of poly(sulfide) domains within the sample. The PCS-75 and PCS-25 copolymers display a complex degradation profile spanning the range of 160 to 500 °C, featuring multiple peaks as illustrated in Fig. S2b. Notably, PCS-25 exhibits up to five peaks. However, complete degradation is not observed in any of the copolymers, indicating considerable stability. To complement the structural characterization of the copolymers, GPC measurements were performed, showing the oligomeric nature with low average molecular weights (<1 KDa) as expected for inverse vulcanization copolymers, see SI Table S1.

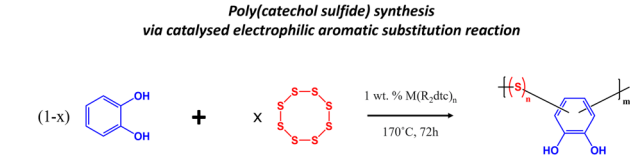

Scheme 1 Synthesis route of PCS copolymers.

Electrochemical characterization of poly(catechol sulfide)

As depicted in Scheme 1, the PCS copolymers might contain two well-known redox moieties, named catechol[21,23,34–36] and poly(sulfide),[13,17,37–41] depending on their chemical composition

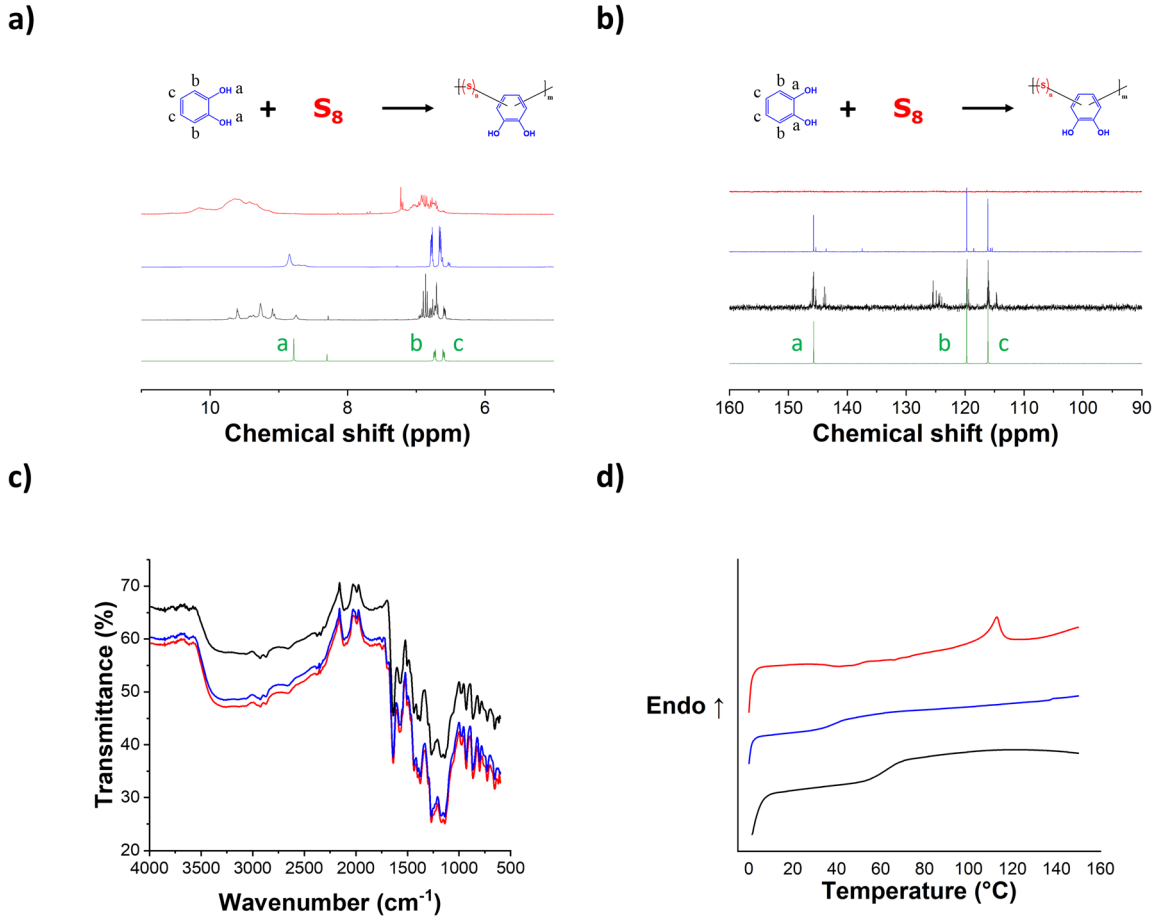

Fig. 1 (a) ^{1}H NMR, (b) ^{13}C NMR, (c) FTIR spectra and (d) DSC curves of catechol (green) and PCS copolymers as a function of sulfur content: 25 wt% (black), 50 wt% (blue) and 75 wt% (red).

Table 1 Thermal properties of PCS copolymers as a function of sulfur content

Sample	T_g (°C)	T_m (°C)	ΔH_m (J g^{-1})
PCS-25	62	—	—
PCS-50	38	—	—
PCS-75	51	113	4

as previously reported, the redox mechanism associated with the catechol moiety is related to the reversible enolization process of carbonyl groups, with a reported formal potential around 3.1 V *vs.* Li/Li^{+}, depending on the electrolyte and molecular design of the catechol compounds.[21,23,34–36] As per their chemical compositions, all PCS copolymers should contain a catechol moiety and thus exhibit a catechol related redox process. On the other hand, the reported redox mechanism for the poly(sulfide) moiety corresponds to the reversible cleavage of S–S bonds, which occurs stepwise in a potential range between 2.3 V and 1.7 V *vs.* Li/Li^{+} as a function of the number of sulfur atom in the poly(sulfide) moiety.[13,17,37,38] It noteworthy that the redox process related to the poly(sulfide) moiety should only occur for the PCS copolymers with a sulfur/catechol molar ratio above 2.[13,17,37,38] Below this sulfur content, there is no sufficient mole of sulfur with respect to the number of moles of catechol in the PCS copolymers to allow the formation of C–S–(S)$_n$–C linkage with $n \geq 1$, and thus the S–S redox process. Based on this criterion, Table 2 summarizes the sulfur/catechol mole ratio and the corresponding theoretical

Table 2 Theoretical capacity of PCS copolymers as a function of sulfur content

Sample	S_8 weight percentage, x [wt%]	S_8/catechol molar ratio (n)	Theoretical capacity (number of electrons, e^{-}) [mAh g^{-1}]
PCS-25	25	1.1	365.1 (2 e^{-})
PCS-50	50	3.4	730.2 (6 e^{-})
PCS-75	75	10.3	1217.0 (20 e^{-})

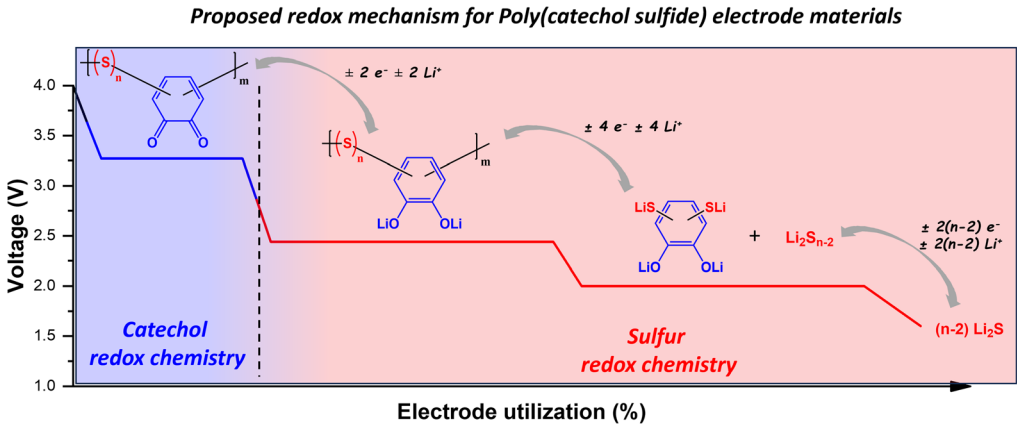

Fig. 2 Illustration of redox processes associated with PCS copolymers.

capacity expected for all PCS copolymers. While PCS-50 and PCS-75 copolymers are expected to display both catechol and poly(sulfide) redox activities, PCS-25 should only exhibit catechol redox activity, due to the lack of C–S–$(S)_n$–C linkage formation with $n > 1$. Fig. 2 illustrates the hypothesised redox process present in the PCS copolymers, as a function of n.

To assess the electrochemical properties of the PCS copolymers, cathode electrodes were formulated using PCS-25 and PCS-75 copolymers as active materials and their electrochemical performances were assessed in lithium metal batteries using a 1 M lithium bis(trifluoro-methanesulfonyl) imide (LiTFSI) solution in 1,3-dioxolane (DOL)/1,2-dimethoxyethane (DME) as the electrolyte. Fig. 3a shows the voltage profiles for the first two formation cycles at a C-rate of C/2. As can be seen in Fig. 3a, the PCS-25 copolymer exhibits only one stable discharge plateau at a voltage of around 3.06 V *vs.* Li/Li^+, which corresponds to the reversible enolization process of the catechol moiety as reported for catechol based redox polymers.[21,35] No discharge plateaus are observed in a voltage range between 2.3 V and 1.7 V *vs.* Li/Li^+, confirming that no poly(-sulfide) redox process (*i.e.* cleavage of S–S bonds) is observed in the PCS-25 copolymer. Interestingly, two charge plateaus are observed at a voltage of around 3.15 V and 3.75 V *vs.* Li/Li^+, respectively. Upon cycling, the former charge plateau becomes more pronounced, while the latter diminishes. Such a phenomenon has been previously reported and is likely associated with a change in the redox couples, going from hydroquinone/quinone to dilithium hydroquinone/quinone, with the later redox couple having a lower redox potential.[34] On the other hand, PCS-75 displays three main discharge plateaus at a voltage of around 3.07 V, 2.25 V and 1.75 V *vs.* Li/Li^+, respectively, as shown in Fig. 3a. The former discharge plateau corresponds to the enolization reaction of the quinone moiety into the dilithium hydroquinone moiety, associated with the catechol moiety. The second plateau is likely associated with the cleavage of the C–S–$(S)_n$–C linkage of PCS copolymers, which could form the dilithium hydroquinone disulfide compound and linear lithium poly(sulfide) compounds (Li_2S_{n-2}), as depicted in Fig. 2.[17,37,38] The latter plateau corresponds to the further reduction of the linear lithium poly(sulfide) into lithium sulfide, through intermediate length lithium poly(sulfide) (Li_2S_{n-x}; with $x > 2$).[17,37,38] Interestingly, only two charge plateaus

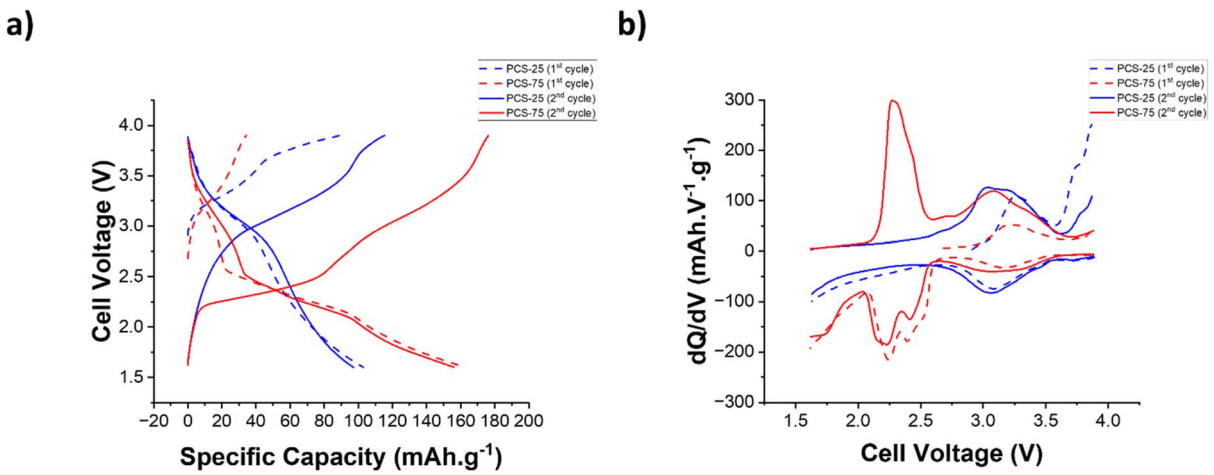

Fig. 3 (a) Voltage profiles and (b) differential capacity (dq/dV) curves from the galvanostatic cycling of lithium metal batteries, with either the PCS-25 (blue) or PCS-75 (red) based cathode, during the first two formation cycles at a C-rate of C/2.

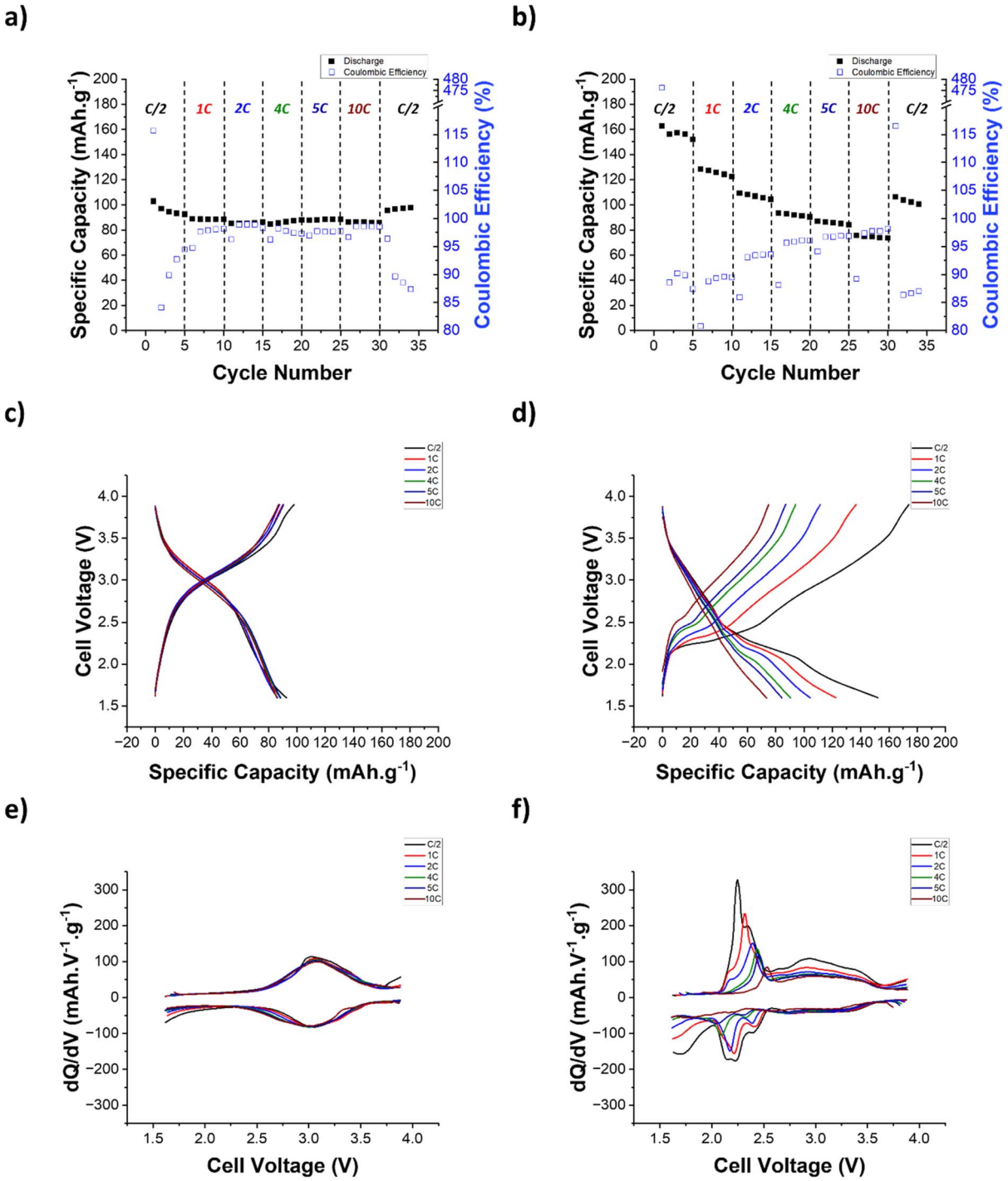

Fig. 4 Galvanostatic cycling of either the PCS-25 (a, c and e) or PCS-75 (b, d and f) based cathode in lithium metal batteries at various C-rates: specific discharge capacity as a function of cycle number (a and b) and the corresponding voltage profiles (c and d) and differential capacity (dq/dV) curves (e and f).

are observed at a voltage of around 2.35 V and 3.10 V *vs.* Li/Li^+, respectively. The former charge plateau is likely associated with the reversible formation of linear lithium poly(sulfide) (Li_2S_{n-2}) and then the C–S–$(S)_n$–C linkage of PCS copolymers. The latter charge plateau corresponds to the oxidation of the dilithium hydroquinone moiety into the quinone moiety.

To further understand the redox processes associated with the PCS copolymers, the differential capacity (dq/dV) curves for the first two formation cycles at a C-rate of C/2 have been also plotted. As can be seen in Fig. 3b for both PCS-25 and PCS-75 copolymers, two waves can be observed for both the oxidation and reduction processes of the catechol moiety, indicating two consecutive steps of a one-electron transfer reaction.[21,23,34–36] As

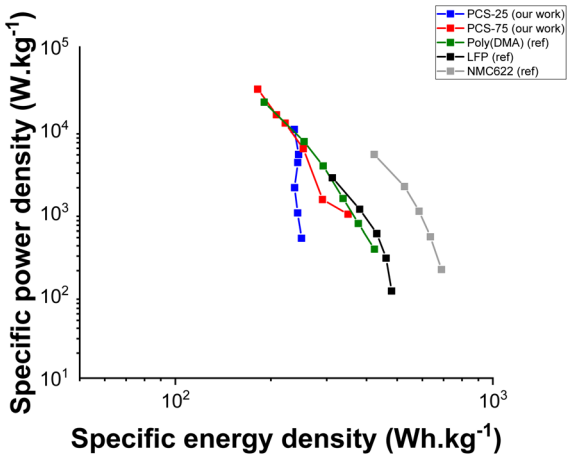

Fig. 5 Comparing the electrochemical performance of both PCS-25 and PCS-75 based cathodes in a Ragone plot with respect to two state-of-the-art inorganic cathode materials (lithium iron phosphate, LFP;[48] lithium nickel manganese cobalt, NMC622 (ref. 49)) and a catechol-based organic electrode material (poly(dopamine methacrylamide), poly(DMA);[35]).

mentioned previously, the PCS-75 copolymer exhibits two additional discharge plateaus, when compared to the PCS-25 copolymer, which were associated with the poly(sulfide) redox process. Interestingly, the former sulfur discharge plateau, located at a voltage of around 2.25 V *vs.* Li/Li^+, is also clearly deconvoluted into two reduction waves in dq/dV curves, suggesting two consecutive steps of two-electron transfer reactions. This could indicate that there is an energy barrier difference between the two S–S bonds that are directly covalently bonded to the catechol moiety (*i.e.* S–S–catechol–S–S), as it is similarly observed for the enolization of the two ketone groups of the anthraquinone-based polymer.[42,43] Alternatively, this two-step transfer reactions could be also the result of the random substitution of the catechol ring in the PCS copolymers (*e.g. ortho*, *para* and/or *meta*), although preference for *ortho* substitution has been reported for similar systems.[44] On the other hand, the second sulfur discharge plateau, located at a voltage of around 1.75 V *vs.* Li/Li^+, results in one reduction wave in dq/dV curves, suggesting one two-electron transfer reaction. This is consistent with the assignment of this discharge plateau to the reduction of the linear lithium poly(sulfide) into lithium sulfide, through intermediate length lithium poly(sulfide) (Li_2S_{n-x}; with $x > 2$). Upon charging, only one charge plateau, located at a voltage of around 2.35 V *vs.* Li/Li^+, could be identified to the poly(sulfide) redox process. The dq/dV curve around this voltage reveals a multicomponent oxidation wave, suggesting the reversible oxidation of the three-reduction poly(-sulfide) processes previously discussed occurs at a voltage range between 2.10 V and 2.55 V *vs.* Li/Li^+, at a C-rate of C/2. More

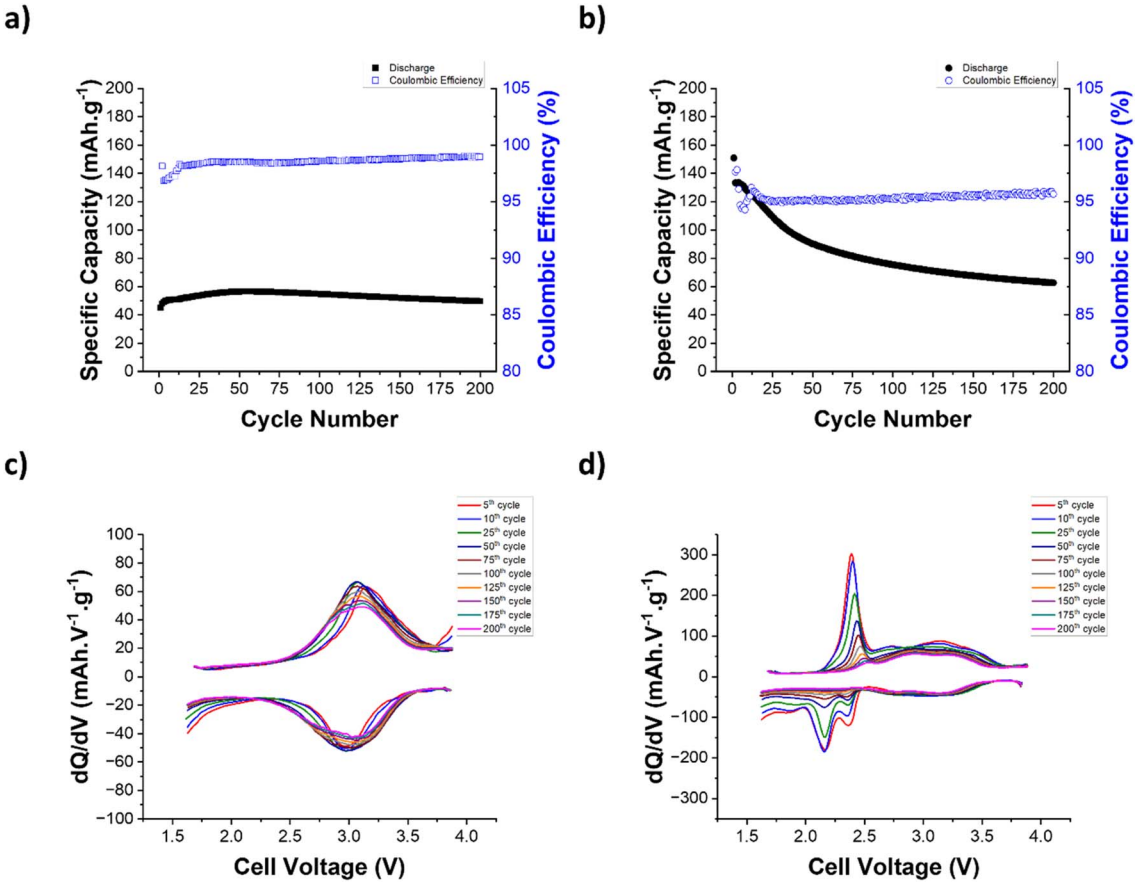

Fig. 6 Long term galvanostatic cycling of either the PCS-25 (a and c) or PCS-75 (b and d) based cathode in lithium metal batteries at a C-rate of 4 C: specific discharge capacity as a function of cycle number (a and b) and the corresponding differential capacity (dq/dV) curves (c and d).

details about these oxidation processes are provided in the following rate capability section.

Poly(catechol sulfide) as cathode materials in organic lithium metal batteries

Once a better understanding of the redox processes of the PCS copolymers was achieved, the rate capability of the cathode formulated using the PCS-25 and PCS-75 copolymers was studied and the results are shown in Fig. 4. At a C-rate of C/2, PCS-25 delivers an initial specific discharge capacity of 103.0 mAh g^{-1} with a coulombic efficiency (CE) of 115.7% for the first cycle, which is only attributed to the catechol redox process (see Fig. 4a). During the first charge cycle, only the oxidation process of the catechol moiety into quinone moiety is expected for all PCS copolymers, as the poly(sulfide) moiety cannot undergo a further oxidation process into elemental sulfur as the poly(sulfide) moiety is covalently bonded to the catechol moiety. The CE above 100% observed in the first cycle of PCS-25 suggests the presence of benzoquinone groups, to a small extent, in the pristine PCS-25 copolymer (*e.g.* the oxidized form of the catechol moiety), which can be then reduced during the first discharge and account for the discharge capacity gain observed in the first cycle. However, it is difficult to confirm the presence of benzoquinone in the PCS copolymer by FTIR and NMR spectroscopies due to the overlap between the νC=O and νC=C bands and the low intensity of quaternary carbon, respectively. Previous reports on the synthesis of sulfide-based polymers support the possible formation of a benzoquinone group during the synthesis.[45–47] Upon cycling at a C-rate of C/2, the CE first dropped to 84.1% on the second cycle and then increased to 94.8% on the fifth cycle, with a specific discharge capacity stabilizing at 92.6 mAh g^{-1}. The observed CE trend supports the possible presence of benzoquinone groups in the pristine PCS-25. Increasing the C-rate from C/2 to 10C results in almost no reduction of the delivered specific discharge capacity (*i.e.*, 86.0%), corresponding to a capacity retention of 92.9%. As can be seen in Fig. 4c and e, no polarization is observed in both the voltage profile and dq/dV curves, highlighting the excellent rate capability of PCS-25. Fig. 4b, d and f show the rate capability results of the PCS-75 copolymer. As can be seen in Fig. 4b, the PCS-75 copolymer delivers a specific discharge capacity of 162.9 mAh g^{-1}, with an initial CE of 476.3% for the first cycle at a C-rate of C/2. This high value of CE is expected for the first cycle as only the oxidation process of the catechol is expected in the as-synthesized PCS-75 copolymer. Further cycling at a C-rate of C/2 reveals that slight capacity fading is observed at a delivered specific discharge capacity of 152.6 mAh g^{-1} with a CE of 87.4% on the fifth cycle. The PCS-75 copolymer exhibits a lower CE when compared to PCS-75 at a C-rate of C/2, suggesting that the poly(sulfide) redox process is not fully reversible. Upon increasing the C-rate from C/2 to 10 C, the PCS-75 copolymer displays a moderate rate capability, with a capacity retention of 48.4%, delivering a specific discharge capacity of 73.6 mAh g^{-1}. Interestingly, the CE increases from 87.4% to 98.2%, when increasing the C-rate from C/2 to 10 C. To further understand the lower rate performance of the PCS-75 copolymer, the voltage profile and dq/dV curves at various C-rates are shown in Fig. 4d and f, respectively. No polarization is observed for the catechol redox process, as for the PCS-25 copolymer. In contrast, strong polarization is observed for the two discharge plateaus associated with the poly(sulfide) redox processes. A cathodic shift of around 250 mV is observed for the two reduction waves derived from the former poly(sulfide) discharge plateau (Fig. 4f). Interestingly, the third poly(sulfide) reduction wave in dq/dV plots, corresponding to the second poly(sulfide) discharge plateau in the voltage profile curves, cathodically shifts outside the voltage range of the battery, when a C-rate superior to that of 2 C is used. This suggests that the reduction of the linear lithium poly(sulfide), which is theoretically the redox process that delivers the most capacity, is not occurring in the PCS-75 copolymer above a C-rate of 2 C. This coincides with the larger proportion of the capacity retention lost (*i.e.*, 78.6%) observed for a C-rate below 4 C. Upon charging at various C-rates, the multicomponent oxidation wave previously observed at a C-rate of C/2 becomes more deconvoluted, suggesting a difference in the oxidation kinetics of the various poly(sulfide) processes. A first oxidation wave, located at a voltage of around 2.2 V, is observed for the C-rate up to 2 C in the dq/dV curves. This is consistent with the cathodic shift of the lithium poly(sulfide) reduction peak outside the voltage range for a C-rate above 2 C. This suggests that this first oxidation wave is related to the oxidation of lithium sulfide into linear lithium poly(sulfide), through intermediate length lithium poly(sulfide) (Li_2S_{n-x}; with $x > 2$). Interestingly, no anodic shift is observed for this oxidation wave, suggesting that the oxidation process has faster kinetics compared to the corresponding reduction process. Similar to their corresponding reduction process, the subsequent two oxidation waves undergo a cathodic shift of around 250 mV, when the C-rate is increased from C/2 to 10 C. This suggests that both the oxidation and reduction processes, corresponding to the reversible cleavage of the C–S–$(S)_n$–C linkage of the PCS-75 copolymer, have similar kinetics. Overall, the results suggest that the poly(sulfide) redox process has a lower rate capability, when compared to the catechol redox process.

To further assess the rate capability of the PCS-25 and PCS-75 copolymers, their specific energy and power densities are displayed in a Ragone plot as shown in Fig. 5. For comparison purpose, the specific energy and power densities of two state-of-the-art inorganic cathode materials (*i.e.* lithium iron phosphate, LFP;[48] lithium nickel manganese cobalt, NMC622 (ref. 49)), used in lithium-ion batteries, as well as a catechol-based organic electrode material (poly(dopamine methacrylamide), poly(-DMA)),[35] were extracted from the aforementioned references and plotted in Fig. 5. It is noteworthy that all specific energy and power densities are normalized by the weight of the electrode active material. As can be seen, the PCS-25 copolymer displays great power density capability, delivering an almost constant specific energy density of 237 Wh kg^{-1} at specific power densities, ranging from 0.49 to 10.17 kW kg^{-1}. Compared to PCS-25, PCS-75 exhibits slightly lower power density capability, with a decrease in specific energy density, from 350 to 182 Wh kg^{-1}, when specific power density is increased from 0.95 to 31.18 kW kg^{-1}. This lower power density capability is associated with the sluggish poly(sulfide) redox process, which provides

minor capacity contribution above a C-rate of 2 C. With respect to the reference catechol-based organic cathode material, PCS-25 displays an improved power density capability, with a constant specific energy density of 237 Wh kg^{-1} at specific power densities ranging from 0.49 to 10.17 kW kg^{-1} compared to poly(DMA), which exhibits a decrease in specific energy density from 424 Wh kg^{-1} to 191 Wh kg^{-1} at a specific power density of 0.36 kW kg^{-1} and 21.70 kW kg^{-1}, respectively. On the other hand, PCS-75 displays lower power density capability than poly(DMA), due to the sluggish poly(sulfide) redox process and a lower catechol content. From the data extracted for the inorganic cathode materials,[48,49] a maximum specific power density of 2.64 kW kg^{-1} and 5.06 kW $kg^{-1}$was achieved for LFP and NMC622, respectively, delivering a specific energy density of 312 Wh kg^{-1} and 423 Wh kg^{-1}, respectively. It is noteworthy that the maximum specific power densities achieved for LFP and NMC622 inorganic cathode materials were obtained at a C-rate of 5 C. Enabling a faster C-rate, and thus specific power density, is a challenging task for inorganic cathode materials.[50] In this respect, both PCS-25 and PCS-75 copolymers are able to deliver higher specific power density of 10.17 kW kg^{-1} and 31.18 kW kg^{-1},respectively, while still delivering a moderate energy density of 237 Wh kg^{-1} and 182 Wh kg^{-1}, respectively. Overall, both PCS-25 and PCS-75 copolymers show great power density capability, highlighting their potential as cathode materials.

Finally, the long-term cycling stability of the PCS-25 and PCS-75 copolymers was assessed at a C-rate of 4 C and the results are shown in Fig. 6. As can be seen, a clear electrode activation process is observed for PCS-25 with a slight increase of the specific discharge capacity delivered during the first 50 cycles, which is also associated with a slight cathodic shift of catechol redox waves in the dq/dV curves. After this activation process, PCS-25 displays outstanding long-term cycling stability, with a capacity retention of 88.0% and a coulombic efficiency of 99.0% after 200 cycles. Such results are superior to those of the reference catechol-based organic cathode material,[35] which achieved a capacity retention of 81% after 200 cycles at a C-rate of 1 C. On the other hand, PCS-75 displays strong capacity fading during the first 100 cycles (*i.e.* 49.9% capacity loss), followed by a second regime with an improved capacity retention (*i.e.*, 8.5% capacity loss). The dq/dV curves reveal that the capacity loss observed in the PCS-75 copolymer is mainly linked with the intensity reduction of redox waves associated with the C–S–$(S)_n$–C linkage of the PCS-75 copolymer, likely due to the dissolution of the linear lithium poly(sulfide) (Li_2S_{n-2}) formed and the subsequent well-known shuttle effect.[50] It is noteworthy that the lithium metal battery constructed using the PCS-75 copolymer is just a proof-of-concept device with no optimized electrolyte (*e.g.* sparingly solvating electrolyte and[51] solid-state electrolyte[52]) and/or separator[53] to inhibit the lithium poly(sulfide) shuttle effect[54] and thus improve capacity retention.

Conclusions

Novel bio-inspired poly(catechol sulfide) copolymers have been synthesized using an environmentally friendly catalytic polymerization method for application as organic cathode materials for lithium metal batteries. The PCS copolymers with varying compositions of catechol and poly(sulfide) were characterized by FTIR, ^1H and ^{13}C NMR. Cyclic voltammetry confirms the dual redox properties of the PCS copolymers when the sulfur content is increased above 25 wt%, below which only the catechol redox group is active. The electrochemical characterization of the PCS-based organic cathode in lithium metal batteries reveals that the catechol redox process exhibits great rate capability and cycling stability, while the poly(sulfide) redox process suffers from more sluggish kinetics due to the nature of the redox process (*i.e.*, bond cleavage) as well as poorer cycling stability due to the dissolution of the linear lithium poly(sulfide), a phenomenon that could be limited through electrolyte optimization (*e.g.*, sparingly solvating electrolyte and solid-state electrolyte). Nevertheless, both PCS-25 and PCS-75 display great specific energy densities of 237 Wh kg^{-1} and 182 Wh kg^{-1} at specific power densities of 10.17 kW kg^{-1} and 31.18 kW kg^{-1}, respectively. These results highlight the potential of PCS copolymers as sustainable and high power and energy density organic cathode materials for lithium metal batteries.

Conflicts of interest

There are no conflicts to declare.

Data availability

The data supporting this article have been included as part of the SI.

GPC and thermal characterization data. See DOI: https://doi.org/10.1039/d5ta04701c.

Acknowledgements

Juan Cubero-Cardoso thanks the Next Generation European Funds and the Ministry of Universities of Spain for funding the Recualificación del Profesorado Universitario system. The authors express their acknowledgement of Fundación Cátedra Cepsa (Moeve) for kindly supplying the sulfur.

References

1 International Energy Agency (IEA), *Batteries and Secure Energy Transitions*, 2024, https://www.iea.org/reports/batteries-and-secure-energy-transitions.
2 European Commission, *Circular economy: New law on more sustainable, circular and safe batteries enters into force*, 2023, https://environment.ec.europa.eu/news/new-law-more-sustainable-circular-and-safe-batteries-enters-force-2023-08-17_en.
3 European Commission, *Critical Raw Materials*, https://single-market-economy.ec.europa.eu/sectors/raw-materials/areas-specific-interest/critical-raw-materials_en.
4 P. Poizot, J. Gaubicher, S. Renault, L. Dubois, Y. Liang and Y. Yao, Opportunities and Challenges for Organic Electrodes in Electrochemical Energy Storage, *Chem. Rev.*, 2020, **120**, 6490–6557.

5 S. Muench, A. Wild, C. Friebe, B. Häupler, T. Janoschka and U. S. Schubert, Polymer-Based Organic Batteries, *Chem. Rev.*, 2016, **116**, 9438–9484.
6 N. Goujon, N. Casado, N. Patil, R. Marcilla and D. Mecerreyes, Organic batteries based on just redox polymers, *Prog. Polym. Sci.*, 2021, **122**, 101449.
7 W. J. Chung, J. J. Griebel, E. T. Kim and J. Pyun, The use of elemental sulfur as an alternative feedstock for polymeric materials, *Nat. Chem.*, 2013, **5**(6), 518–524.
8 B. Zheng, L. Zhong, X. Wang and H. Zhang, Structural evolution during inverse vulcanization, *Nat. Commun.*, 2024, **15**(1), 1–17.
9 A. Haro-Martínez, R. Arroyo-Carrasco, L. Galván and J. Urbano, Competitive and synergistic effects of metal adsorption in water remediation processes mediated by hybrid copolymers, *Chem. Eng. J.*, 2023, **470**, 143905.
10 A. Alex, N. K. Singha and S. Choudhury, Exploring inverse vulcanization in lithium–sulfur batteries, *Curr. Opin. Electrochem.*, 2023, **39**, 101271.
11 M. Vera-Tuset, R. Mas-Ballesté, I. Cuadrado, A. Moya and S. Bruña, Electroactive sulfur-rich materials obtained *via* inverse vulcanization of a diallylsilyl-functionalized ferrocene, *Polym. Chem.*, 2024, **15**, 1015–1025.
12 Z. Chen, J. Droste, G. Zhai, J. Zhu, J. Yang, M. R. Hansen and X. Zhuang, Sulfur-anchored azulene as a cathode material for Li–S batteries, *Chem. Commun.*, 2019, **55**, 9047–9050.
13 I. Gomez, O. Leonet, J. Alberto Blazquez, H.-J. Grande and D. Mecerreyes, Poly(anthraquinonyl sulfides): High Capacity Redox Polymers for Energy Storage, *ACS Macro Lett.*, 2018, **7**, 419–424.
14 M. Liu, S. J. Visco and L. C. De Jonghe, Electrochemical Properties of Organic Disulfide/Thiolate Redox Couples, *J. Electrochem. Soc.*, 1989, **136**, 2570–2575.
15 M. Liu, S. J. Visco and L. C. De Jonghe, Novel Solid Redox Polymerization Electrodes: All-Solid-State, Thin-Film, Rechargeable Lithium Batteries, *J. Electrochem. Soc.*, 1991, **138**, 1891–1895.
16 Y. Li, H. Zhan, L. Kong, C. Zhan and Y. Zhou, Electrochemical properties of PABTH as cathode materials for rechargeable lithium battery, *Electrochem. Commun.*, 2007, **9**, 1217–1221.
17 S. R. Deng, L. B. Kong, G. Q. Hu, T. Wu, D. Li, Y. H. Zhou and Z. Y. Li, Benzene-based polyorganodisulfide cathode materials for secondary lithium batteries, *Electrochim. Acta*, 2006, **51**, 2589–2593.
18 H. Shen, H. Qiao and H. Zhang, Sulfur-urushiol copolymer: A material synthesized through inverse vulcanization from renewable resources and its latent application as self-repairable and antimicrobial adhesive, *Chem. Eng. J.*, 2022, **450**, 137905.
19 H. Shen, B. Zheng and H. Zhang, A Decade Development of Inverse Vulcanization Towards Green and Sustainable Practices, *Polym. Rev.*, 2024, **64**(4), 1211–1266.
20 Z. Tang, X. Lin, M. Yu, J. Yang, S. Li, A. K. Mondal and H. Wu, A review of cellulose-based catechol-containing functional materials for advanced applications, *Int. J. Biol. Macromol.*, 2024, **266**, 131243.
21 N. Patil, A. Aqil, F. Ouhib, S. Admassie, O. Inganäs, C. Jérôme and C. Detrembleur, Bioinspired Redox-Active Catechol-Bearing Polymers as Ultrarobust Organic Cathodes for Lithium Storage, *Adv. Mater.*, 2017, **29**, 1–9.
22 N. Patil, A. Mavrandonakis, C. Jérôme and R. Marcilla, High-performance all-organic aqueous batteries based on a poly(imide) anode and poly(catechol) cathode, *J. Mater. Chem. A*, 2021, **9**, 505–514.
23 N. Patil, A. Mavrandonakis, C. Jérôme, C. Detrembleur, J. Palma and R. Marcilla, Polymers Bearing Catechol Pendants as Universal Hosts for Aqueous Rechargeable H + , Li-Ion, and Post-Li-ion (Mono-, Di-, and Trivalent) Batteries, *ACS Appl. Energy Mater.*, 2019, **2**, 3035–3041.
24 N. A. Lundquist, A. D. Tikoalu, M. J. H. Worthington and J. M. Chalker, Reactive Compression Molding Post-Inverse Vulcanization: A Method to Assemble, Recycle, and Repurpose Sulfur Polymers and Composites, *Chem.–Eur. J.*, 2020, **26**, 10035–10044.
25 L. J. Dodd, Ö. Omar, X. Wu and T. Hasell, Investigating the Role and Scope of Catalysts in Inverse Vulcanization, *ACS Catal.*, 2021, **11**, 4441–4455.
26 J. Cubero-Cardoso, A. A. Cuadri, F. G. Fermoso, J. E. Martín-Alfonso and J. Urbano, Promising Chalcogenide Hybrid Copolymers for Sustainable Applications as Bio-lubricants and Metal Adsorbents, *ACS Appl. Polym. Mater.*, 2022, **4**, 3667–3675.
27 J. Cubero-Cardoso, P. Gómez-Villegas, M. Santos-Martín and J. Urbano, Combining vegetable oils and bioactive compounds *via* inverse vulcanization for antioxidant and antimicrobial materials, *Polym. Test.*, 2022, **109**, 107546.
28 A. Haro-martínez, R. Arroyo-carrasco, L. Galván and J. Urbano, Competitive and synergistic effects of metal adsorption in water remediation processes mediated by hybrid copolymers, *Chem. Eng. J.*, 2023, **470**, 143905.
29 X. Zhang, H. Lin, Y. Hu, D. Ding, F. Cai and Y. Wu, Electric tree intrinsic self-healing epoxy insulating materials based on disulfide bond, *Polym. Degrad. Stab.*, 2023, **218**, 110567.
30 R. M. Fitch and D. C. Helgeson, Preparation and thermal properties of organic polysulfide polymers with uniform repeating units, *J. Polym. Sci., Polym. Symp.*, 1969, **22**, 1101–1115.
31 J. Wreczycki, D. M. Bieliński, M. Kozanecki, P. Maczugowska and G. Mlostoń, Anionic Copolymerization of Styrene Sulfide with Elemental Sulfur (S8), *Materials*, 2020, **13**, 2597.
32 I. Gomez, D. Mecerreyes, J. A. Blazquez and L. Rodriguez-Martinez, Inverse vulcanization of sulfur with divinylbenzene: Stable and easy processable cathode material for lithium-sulfur batteries, *J. Power Sources*, 2016, **329**, 72–78.
33 H. Berk, M. Kaya, M. Topcuoglu, N. Turkten, Y. Karatas and A. Cihaner, Synthesis, characterization and application of high sulfur content polymeric materials from fatty acids, *React. Funct. Polym.*, 2023, **187**, 105581.
34 K. Pirnat, N. Casado, L. Porcarelli, N. Ballard and D. Mecerreyes, Synthesis of Redox Polymer Nanoparticles Based on Poly(vinyl catechols) and Their Electroactivity, *Macromolecules*, 2019, **52**, 8155–8166.

35 A. Gallastegui, D. Minudri, N. Casado and D. Mecerreyes, Proton trap effect on catechol–pyridine redox polymer nanoparticles as organic electrodes for lithium batteries, *Sustain. Energy Fuels*, 2020, **4**, 3934–3942.

36 A. Gallastegui, O. Camara, D. Minudri and D. Mecerreyes, Aging Effect of Catechol Redox Polymer Nanoparticles for Hybrid Supercapacitors, *Batteries Supercaps*, 2022, **5**, e202200155.

37 M. B. Preefer, B. Oschmann, C. J. Hawker, R. Seshadri and F. Wudl, High Sulfur Content Material with Stable Cycling in Lithium-Sulfur Batteries, *Angew. Chem., Int. Ed.*, 2017, **56**, 15118–15122.

38 C. Sonnenschein, C. P. Ender, F. Wang, D. Schollmeyer, X. Feng, A. Narita and K. Müllen, Oligophenyls with Multiple Disulfide Bridges as Higher Homologues of Dibenzo[c,e][1,2]dithiin: Synthesis and Application in Lithium-Ion Batteries, *Chem.–Eur. J.*, 2020, **26**, 8007–8011.

39 Y. Gong, J. Li, K. Yang and Y. Zhao, Towards Practical Application of Li–S Battery with High Sulfur Loading and Lean Electrolyte: Will Carbon-Based Hosts Win This Race?, *Nano-Micro Lett.*, 2023, **15**(1), 1–39.

40 X. Zhang, W. Guo and Y. Fu, Hybrid Organosulfur Cathode Materials for Rechargeable Lithium Batteries, *Acc. Mater. Res.*, 2024, **5**, 316–328.

41 S. Xin, L. Gu, N. H. Zhao, Y. X. Yin, L. J. Zhou, Y. G. Guo and L. J. Wan, Smaller sulfur molecules promise better lithium'sulfur batteries, *J. Am. Chem. Soc.*, 2012, **134**, 18510–18513.

42 Z. Song, H. Zhan and Y. Zhou, Anthraquinone based polymer as high performance cathode material for rechargeable lithium batteries, *Chem. Commun.*, 2009, 448–450.

43 W. Xu, A. Read, P. K. Koech and J. G. Zhang, Factors affecting the battery performance of anthraquinone-based organic cathode materials, *J. Mater. Chem.*, 2012, **22**, 4032–4039.

44 M. Karayilan, T. S. Kleine, K. J. Carothers and J. Pyun, Chalcogenide hybrid inorganic/organic polymer resins: Amine functional prepolymers from elemental sulfur, *J. Polym. Sci., Part A: Polym. Chem.*, 2019, **58**, 35–41.

45 Z. Song, Y. Qian, T. Zhang and M. Otani, Poly(benzoquinonyl sulfide) as a High-Energy Organic Cathode for Rechargeable Li and Na Batteries, *Adv. Sci.*, 2015, **2**, 1500124.

46 J. Xie, Z. Wang, Z. J. Xu and Q. Zhang, Toward a High-Performance All-Plastic Full Battery with a'Single Organic Polymer as Both Cathode and Anode, *Adv. Energy Mater.*, 2018, **8**, 1703509.

47 R. Narayan, A. Blagojević, G. Mali, J. F. Vélez Santa, J. Bitenc, A. Randon-Vitanova and R. Dominko, Nanostructured Poly(hydroquinonyl-benzoquinonyl sulfide)/Multiwalled Carbon Nanotube Composite Cathodes: Improved Synthesis and Performance for Rechargeable Li and Mg Organic Batteries, *Chem. Mater.*, 2022, **34**, 6378–6388.

48 F. Li, Y. Gong, G. Jia, Q. Wang, Z. Peng, W. Fan and B. Bai, A novel dual-salts of LiTFSI and LiODFB in LiFePO4-based batteries for suppressing aluminum corrosion and improving cycling stability, *J. Power Sources*, 2015, **295**, 47–54.

49 L. Xu, F. Zhou, J. Kong, Z. Chen and K. Chen, Synthesis of $Li(Ni_{0.6}Co_{0.2}Mn_{0.2})O_2$ with sodium DL-lactate as an eco-friendly chelating agent and its electrochemical performances for lithium-ion batteries, *Ionics*, 2018, **24**, 2261–2273.

50 M. Weiss, R. Ruess, J. Kasnatscheew and J. Janek, Fast Charging of Lithium-Ion Batteries: A Review of Materials Aspects, *Adv. Energy Mater.*, 2021, **11**, 2101126.

51 A. Manthiram, Y. Fu, S. H. Chung, C. Zu and Y. S. Su, Rechargeable lithium-sulfur batteries, *Chem. Rev.*, 2014, **114**, 11751–11787.

52 L. Cheng, L. A. Curtiss, K. R. Zavadil, A. A. Gewirth, Y. Shao and K. G. Gallagher, Sparingly Solvating Electrolytes for High Energy Density Lithium-Sulfur Batteries, *ACS Energy Lett.*, 2016, **1**, 503–509.

53 D. Wang, L. J. Jhang, R. Kou and D. Wang, Realizing high-capacity all-solid-state lithium-sulfur batteries using a low-density inorganic solid-state electrolyte, *Nat. Commun.*, 2023, **14**(1), 1–10.

54 J. Wang, H. Wang, S. Jia and X. Li, Recent advances in inhibiting shuttle effect of polysulfide in lithium-sulfur batteries, *J. Energy Storage*, 2023, **72**, 108372.

